Probabilistic Exposure Risk Assessment with Advective-Dispersive Well Vulnerability Criteria

Rainer Enzenhoefer[a,*], Wolfgang Nowak[a], Rainer Helmig[a]

[a]*Institute of Hydraulic Engineering, Department of Hydromechanics and Modeling of Hydrosystems, University of Stuttgart, Pfaffenwaldring 61, D - 70569 Stuttgart, Germany*

Abstract

Time-related advection-based well-head protection zones are commonly used to manage the contamination risk of drinking water wells. According to current Water Safety Plans, catchment managers and stakeholders need more information for advanced risk management to better control and monitor all possible hazards within catchments. The goal of this work is to cast the four advective-dispersive intrinsic well vulnerability criteria by Frind et al. [1] into a framework of probabilistic risk assessment. These criteria are the (i) arrival time and (ii) level of peak concentration, (iii) time until first arrival of critical concentrations and (iv) exposure time. Our probabilistic framework yields catchment-wide maps that show the probability to exceed critical values for each of these criteria. This provides indispensable information for catchment managers and stakeholders to perform probabilistic exposure risk assessment and so improves the basis for risk-informed well-head management.

*Corresponding author
Email address: `rainer.enzenhoefer@iws.uni-stuttgart.de` (Rainer Enzenhoefer)
URL: `http://www.hydrosys.uni-stuttgart.de/institut/mitarbeiter/person.en.php?name=1234` (Rainer Enzenhoefer)

We separate the uncertainty of plume location and actual dilution by resolving heterogeneity with high-resolution Monte Carlo simulations. To keep computational costs low, we adopt a reverse transport formulation, and combine it with the temporal moment approach for model reduction. We recover the time-dependent breakthrough curves and well vulnerability criteria from the temporal moments by Maximum Entropy reconstruction in log-time.
Our method is independent of dimensionality, boundary conditions and can account for arbitrary sources of uncertainty. It can be coupled with any method for conditioning on available data. For simplicity, we demonstrate the concept on a 2D example, using the Bayesian version of the Generalized Likelihood Uncertainty Estimator (GLUE) for conditioning on synthetic data.
Keywords: well catchment delineation, groundwater protection, well vulnerability, risk assessment, uncertainty, Bayesian GLUE

---

1. Introduction

The increasing demand on safe drinking water and the risks posed by groundwater contamination lead to a conflict between interests of economics and the goal to maintain high standards in water quality. As early as in 1975, the US Nuclear Regulatory Commission [2] required to perform probabilistic risk assessment (PRA) for nuclear power plants. A decade later, the US Environmental Protection Agency (EPA) started to give risk assessment guidance for Superfund sites in groundwater engineering [3]. In 2004, the World Health Organization (WHO) [4] stated within their drinking water guideline, that "Drinking-water quality is an issue of concern for human health in developing and developed countries world-wide". They recommend using groundwater protection management schemes in order to ensure clean and safe drinking water via implementing Water Safety Plans (WSP) [5] into legislation. The fully applied Water Safety Plans aim to know *(1) what kind of hazards exist within the water catchment, (2) how these hazards can be controlled and (3) knowing that they are controlled*. The WSP will most probably be part of the upcoming revision of the European Council Directive 98/83/EC [6], forcing water managers to perform risk management and to take risk-based decisions for pumping safe drinking water.

A classical approach for risk control is to delineate time-related well-head protection areas by calculating hypothetical travel-time zones in a deterministic fashion, as suggested by the US EPA [7]. Evers and Lerner [8] pointed out the importance of asking the question: How uncertain is our estimate of well-head protection zones? Unfortunately, each model is just an idealization of the real world, taking a set of assumptions and approximations for modeling a physical subsystem. These assumptions include, among others, initial and boundary conditions, discretization schemes, or even simplistic mathematical descriptions of the observed or unobserved physical behavior. This inevitably invokes the problem of model uncertainty, leading engineers and scientists to ask the question which model alternative represents reality best (e.g., Neuman [9], Hoeting et al. [10] and Park et al. [11]). Additionally, the lack of knowledge about the subsurface, heterogeneity and the scarcity of data lead to uncertainty in material properties. These uncertainties affect physical subsurface processes such as dilution and spreading of contaminant plumes to a large extent (e.g., Rubin [12]).

Aven [13] states that "uncertainty analysis constitutes an integral aspect of the risk analysis". It is therefore indispensable to cast the question of well safety and related risks into a probabilistic framework, admit and quantify uncertainty, perform probabilistic risk analysis, and finally seek for conditioning or data assimilation tools to reduce epistemic uncertainty as far as possible (e.g., Feyen et al. [14]).

Varljen and Shafer [15] were the first to use random space functions for the hydraulic conductivity K in order to delineate well capture zones probabilistically, performing conditional Monte Carlo simulations. Other early work in this field was done, for example, by Franzetti and Guadagnini [16] and by van Leeuwen et al. [17]. Many more studies followed, such as Jacobson et al. [18] using analytical, Stauffer et al. [19] using semi-analytical and Vassolo et al. [20], Feyen et al. [14] and Moutsopoulos et al. [21] using numerical approaches to delineate well capture zones while considering uncertainty. The uncertainty in delineating well-head protections areas is, of course, expressed by probability density functions. Cole and Silliman [22] expressed the uncertainty in capture zone location by "percentile capture contours", whereas Guadagnini and Franzetti [23] introduced the concept of "probabilistic isochrones".

Delineating well capture zones most commonly relies on purely advective transport considerations, e.g., based on forward or backward particle tracking (Pollock [24], Moutsopoulos et al. [21]). We see several disadvantages with purely advective approaches: (1) hydromechanical dispersion is neglected, although it leads to dilution of peak concentrations and natural attenuation, and allows contaminants to move across the bounding streamlines. Therefore, purely advective approaches form only a poor basis for risk assessment. (2) The computational effort when using large particle numbers to finely resolve the capture zone outline (e.g., Tosco et al. [25]) is substantial and may become prohibitive for large catchments.

In view of these limitations, Frind et al. [1] introduced four well vulnerability criteria, based on *advective and dispersive* transport considerations. These criteria consider the dilution of potential spill events due to dispersive mechanisms. They also deliver additional information for well catchment managers and stakeholders, such as mean breakthrough or peak arrival time, peak concentration levels or well down time (see Section 2.2 for more details).

To account for the effects of heterogeneity in solute transport, Frind et al. [1] used a macrodispersion approach (e.g., Gelhar and Axness [26], Dagan [27]). One disadvantage of macrodispersion is that it cannot distinguish between the uncertainty in plume location and the actual dilution of the plume. Under non-ergodic transport conditions, the macrodispersion approach fails to capture peak concentrations (e.g., Andricevic and Cvetkovic [28]) and thus will not accurately reflect the risk of well contamination. This is due to spatial integration over irregular plume outlines (spreading) and ensemble averaging over uncertain plume positions. The only exceptions are at the limits of large plumes at late travel times (e.g., Dagan [27], Dentz et al. [29]). In the context of intrinsic well vulnerabilities, dilution is a key factor. It represents the decrease of peak concentrations as mass is distributed over larger volumes (e.g., Kitanidis [30]). This process is primarily influenced by local-scale (hydrodynamic) dispersion and pore-scale diffusion. Therefore, we argue that it is necessary to separate dilution from spreading and from the uncertainty of the plume location in probabilistic well exposure risk assessment, and will do so within our approach (see Section 2).

In risk management, the risk of failure of not to meet the risk objective (here: pumping safe drinking water) is characterized by the magnitude of the adverse effects (e.g., contaminant levels) and the corresponding likelihood of occurrence. In this study, we address the uncertainty of intrinsic well vulnerability criteria (see Section 3.3) via vulnerability isopercentiles (VIPs). We will characterize the latter by the probability to exceed critical values of well vulnerability criteria, leading to VIP maps within the entire catchment. Therefore, the necessary information for probabilistic exposure risk assessment can easily be derived from our VIPs.

Considering human health risk also requires toxicity assessment, taking all possible pathways of ingestion, dermal contact, etc. into account (e.g., Oberg and Bergback [31], Cushman et al. [32], US EPA [3]). The resulting health risk is always specific to individual contaminants and would be, of course, also uncertain. Considering uncertainty in health related parameters is discussed, e.g., by de Barros and Rubin [33], de Barros et al. [34] and de Barros et al. [35]. In contrast, vulnerability criteria such as the ones by Frind et al. [1] are called *intrinsic* because they do not include contaminant-specific sorption, degradation and toxicity factors, but solely focus on the aquifer's general transport properties between contaminant spill location and the pumping well. They can easily be embedded into the multi-barrier context, where they would stand for the transport segment within the aquifer (see Frind et al. [1]). They also provide the basic (conservative) transport information that is for all possible contaminants under consideration, which can be used to reconstruct specific reactive and retarded transport information with smart and relatively simply approaches (e.g., Cirpka and Valocchi [36]). Thus, if cast into an adequate probabilistic framework, the four criteria fully account for the key questions posed by the Water Safety Plans, which are needed by drinking water managers and stakeholders for risk-based decisions within the catchment. This makes our proposed VIPs the fundamental and most essential basis for exposure risk assessment in actively managed well-head protection areas.

2. Approach

2.1. Goals and Approach

The goal of this study is to cast the intrinsic well vulnerability criteria by Frind et al. [1] into a probabilistic framework, while separating between actual dilution and uncertainty in plume spreading and location. The presented work is a combination of Frind et al. [1], Neupauer and Wilson [37], Harvey and Gorelick [38] and Feyen et al. [39]. The novel combination of these building blocks (see Fig. 1) will be explained in the following. The corresponding equations are provided in Section 3.

In order to distinguish between the uncertainty in plume location and actual dilution, we use Monte Carlo simulations that resolve spatial heterogeneity while using local-scale dispersivities. In block (1a) of Fig. 1, Monte Carlo methods lead to cumulative distribution functions instead of just statistical moments. This is also the reason why the US EPA [40] proposes their use in probabilistic risk assessment. This enables us to calculate maps of vulnerability isopercentiles, i.e., each point in the catchment will be assigned a probability that a given critical level of vulnerability is exceeded.

In order to reduce uncertainty, one can couple Monte Carlo simulations with any kind of conditioning schemes in block (1b) of Fig. 1, such as the Bayesian GLUE (e.g., Feyen et al. [41]), Ensemble Kalman Filters for parameter estimation (e.g., Nowak et al. [42]), Markov-Chain-Monte Carlo methods (e.g., Zanini and Kitanidis [43]), the Quasi-linear geostatistical approach (e.g., Kitanidis [44]) and upgrades (e.g., Nowak and Cirpka [45]) or many other methods (e.g., Alcolea et al. [46], Franssen et al. [47]). Because there are many possibilities, each with specific advantages and disadvantages (see, e.g., Franssen et al. [48]), we kept our probabilistic well vulnerability concept independent of the actual choice for the conditioning method. In the illustrative synthetic example provided in Section 4, we will choose the Bayesian version of the GLUE (e.g., Feyen et al. [39]) due to its large flexibility.

Computational costs are the major disadvantage of Monte Carlo. To reduce the computational effort, we will invoke a model reduction based on temporal moments in combination with the reverse formulation of advective-dispersive transport after Neupauer and Wilson [37] (block (2) in Fig. 1). The reverse formulation can calculate capture zones in a most efficient way in situations where contaminant spills could occur anywhere within the domain. The reason is that it delivers the required information about solute transport from all possible spill locations in a single transport simulation. Instead of releasing a solute tracer at each location $\mathbf{x}_i$ within the domain and then solving many separate transport simulations within the same flow field, it reverses the direction of flow and injects a virtual tracer into the groundwater well that is now pumping into the aquifer. The reverse modeling approach is formally based on the adjoint-state solution of solute transport and is conceptually similar to backward particle tracking (e.g., Uffink [49], Frind et al. [1]).

Harvey and Gorelick [38] showed that it is possible to simulate temporal characteristics of transport with moment generating equations (see Fig. 2). Here we apply their method to the reverse formulation. Information on the physical meaning of temporal moments is provided by Cirpka and Kitanidis [50]. The major advantage of using temporal moments is the dramatic gain in computational efficiency in comparison to transient transport calculations. As a drawback, steady state velocity has to be assumed. However, according to Reilly and Pollock [51], this is only a small disadvantage, because seasonal variations are of minor importance for catchment delineation.

In order to evaluate intrinsic well vulnerability criteria, the full time behavior of breakthrough curves (BTC) has to be reconstructed from their temporal moments (block (3) in Fig. 1). Harvey and Gorelick [38] proposed the use of the method of Maximum Entropy in log-time to reconstruct breakthrough curves from moments. Among all reconstruction options, the maximum entropy principle assumes as little as possible and is therefore the least subjective way of reconstruction (e.g., Jaynes [52], Woodbury and Ulrych [53]).

The major advantage of our overall approach is that it is conceptually simple. It only needs minimal code development, and it is fully compatible with commercial simulation software, where no source codes can be intruded or modified. Furthermore, it can be applied to arbitrarily complex problems that include any kind of model uncertainty, uncertainty in boundary conditions, geostatistical assumptions, non-stationarity, and all other sources of uncertainty that might be important to consider in PRA (e.g., Oberg and Bergback [31]).

2.2. Well Vulnerability Criteria in a Risk Context

The four intrinsic well vulnerability criteria defined by Frind et al. [1] (see Fig. 2) are:

1. The time between a spill event and arrival at the well, where Frind et al. [1] used bulk arrival time t_{50} and we will use peak arrival time t_{peak} instead (see discussion in Section 5.2);
2. The level of peak concentration c_{peak} relative to the spill concentration c_{spill};
3. The time t_{crit} to breach a given threshold concentration c_{crit} (e.g., a drinking-water standard); and
4. The time of exposure t_{exp} during which the threshold concentration is exceeded.

We will now reconsider these criteria within the new probabilistic context. The first criterion t_{peak} represents the most common time-related capture delineation scheme. For example, German guidelines [54] state, that the critical travel time to ensure microbiological safety of drinking water is $t = 50\, days$. By original definition, the capture zone is delineated according to the arrival of bulk concentration, often denoted as t_{50}. Here we consider the arrival time of the peak instead, because the often observed tailing of breakthrough curves typically leads to earlier peak arrival t_{peak} than bulk arrival t_{50} in heterogeneous media (see later discussion Section 5). Therefore, we believe that t_{peak} is the more conservative and relevant criterion. Knowing the probability distribution of t_{peak} delivers the information necessary to assess the risk of not meeting the legal regulation about time-related delineation. This allows to rationally choose larger catchment outlines for safety reasons.

The second criterion, peak concentration c_{peak}, accounts for dilution of peak concentrations by pore-scale dispersion, heterogeneity and direct dilution within the pumping well. As discussed in the introduction, assessing this criterion excludes all macrodispersive approaches, because they fail to reflect actual levels and arrival times of peak concentrations. Knowing the statistics of c_{peak} forms the basis for human health risk assessment for acute doses, and allows to judge the compliance with legal threshold concentrations.

In environmental or human health risk assessment, not only the arrival and level of peak concentration itself is of interest, but also whether, at which time and how long a given maximum allowable concentration limit c_{crit} (e.g. a drinking water standard) is breached. The third criterion t_{crit} tells water managers the time available to react before critical contaminant levels are breached at the well. This is the most important information to design early-alert sensor or monitoring systems, and to plan emergency measures, even for worst-case most early arrival on any desirable confidence level.

The fourth criterion, the time t_{exp} above a certain critical concentration level, is equivalent to well down time. It can serve as a measure for damage in economic risk analysis, that a catchment manager lest the water supply company has to cope with. The time out of operation can then easily be expressed monetarily, and the expected financial loss can be compared to the costs of alternative risk treatment methods (see ISO/IEC: 31010 [55]) within risk-informed management decisions. If a spill remains undetected, t_{exp} is also an important impact factor to chronic health risk types.

3. Mathematical Formulation

3.1. Governing Equations

The groundwater flow equation at steady state is

$$-\nabla \cdot (K\,\nabla\phi) = q_s \quad \text{in } \Omega \tag{1}$$

with hydraulic conductivity $K(x)$, hydraulic head ϕ, the source and sink term q_s (including wells) and the domain Ω. A general set of boundary conditions for Eq. (1) is:

$$\begin{aligned} -\left(K\,\nabla\phi\right)\cdot\mathbf{n} &= \hat{q} \quad \text{on } \Gamma_1, \\ \phi &= \hat{\phi} \quad \text{on } \Gamma_2 \end{aligned} \tag{2}$$

Here $\hat{q}$, and $\hat{\phi}$ are prescribed fluxes and heads on the defined boundaries $\Gamma = \Gamma_1 \cup \Gamma_2$ of the domain Ω, respectively, and $\mathbf{n}$ is the normal vector pointing outward of the domain.

Considering a conservative tracer for intrinsic conditions, transport is governed by:

$$\frac{\partial c}{\partial t} + \nabla \cdot (\mathbf{v}c - \mathbf{D}\,\nabla c) = 0 \qquad \text{in}\,\Omega \tag{3}$$

Here c is concentration, t is time, $\mathbf{D}$ is the hydrodynamic dispersion tensor according to Scheidegger [56], velocity $\mathbf{v} = \mathbf{q}/n_e$, $\mathbf{q} = -K\nabla\phi$ is the Darcy velocity, and n_e is the effective porosity. Boundary conditions regarding Eq. (3) are

$$\begin{aligned} -\mathbf{n}\cdot\mathbf{v}c + \mathbf{n}\cdot(\mathbf{D}\,\nabla c) &= 0 \quad \text{on}\ \Gamma \setminus \Gamma_2 \\ c &= \hat{c} \quad \text{on}\ \Gamma_2 \\ -\mathbf{n}\cdot\mathbf{v}c + \mathbf{n}\cdot(\mathbf{D}\,\nabla c) &= -\mathbf{n}\cdot\mathbf{v}\hat{c}_{spill}\delta(t_0) \quad \text{on}\ \Gamma_{x_0} \end{aligned} \tag{4}$$

with $\hat{c}$ being the prescribed concentrations, here $\hat{c} = 0$, on Γ_2. $\hat{c}_{spill}\delta(t_0)$ is an instantaneous contaminant release at time t_0 with concentration $\hat{c}_{spill}$, here localized to a small element inside the domain Ω at the location $\mathbf{x_0}$, enclosed by the internal boundary Γ_{x_0}. For generality, we use a unitless normalized spill concentration of unity. No-flow conditions on all boundaries except $\Gamma \setminus \Gamma_2 \cup \Gamma_{x_0}$ have been assumed here for simplicity of notation.

Instead of solving Eq. (3) and Eq.(4) for many potential spill locations $\mathbf{x_0}$, we consider a reverse flow field $-\mathbf{v}$ and introduce an instantaneous contaminant injection at the well. The transport is subsequently solved reversely, using

$$\frac{\partial c}{\partial t} = \nabla \cdot (\mathbf{v}c + \mathbf{D} \cdot \nabla c) \qquad \text{in}\,\Omega \tag{5}$$

and the boundary conditions change to

$$\begin{aligned} \mathbf{n} \cdot \mathbf{v}c + \mathbf{n} \cdot (\mathbf{D}\,\nabla c) &= 0 \quad \text{on } \Gamma \setminus \Gamma_2 \\ c &= \hat{c} \quad \text{on } \Gamma_2 \\ \mathbf{n} \cdot \mathbf{v}c + \mathbf{n} \cdot (\mathbf{D}\,\nabla c) &= \mathbf{n} \cdot \mathbf{v}\hat{c}_{spill}\delta(t_0) \quad \text{on } \Gamma_{well} \end{aligned} \tag{6}$$

where Γ_{well} is an internal boundary that encloses the well, and $\mathbf{n} \cdot \mathbf{v}$ is the velocity perpendicular to Γ_{well}. More explanation for the backward transport approach is given, e.g., by Uffink [49] and by Neupauer and Wilson [57].

3.2. Temporal Moment Approach

The k-th temporal moment m_k of a breakthrough curve $c(\mathbf{x}, t)$ at location $\mathbf{x}$ is defined as:

$$m_k(\mathbf{x}) = \int_0^\infty t^k \cdot c(\mathbf{x},\, t)\, \mathrm{d}t \tag{7}$$

The zeroth moment m_0 represents the accumulated mass over time that passes by a location $\mathbf{x}$. The normalized first temporal moment m_1/m_0 represents the mean arrival time of a solute at location $\mathbf{x}$. The normalized second central temporal moment m_{2c}/m_0 can be interpreted as local dilution. The physical meaning of several lower-order temporal moments is discussed in more detail by Cirpka and Kitanidis [50]. Higher order temporal moments describe characteristics such as skewness, peakedness, and more complex characteristics of the temporal breakthrough curve's time behavior that are also known from statistics (Wackerly et al. [58]). These characteristics are illustrated in Fig. 2.

Moment generating equations can be derived from Eq. (3) or Eq. (5) and their respective boundary conditions by multiplying the equations with t^k and then integrating over time as in Eq. (7) (Cirpka and Kitanidis [50]). For Eq. (5), partial integration leads to:

$$
\begin{aligned}
\nabla \cdot (\mathbf{v} m_0 + \mathbf{D}\, \nabla m_0) &= 0 \quad \text{for } k = 0 \\
\nabla \cdot (\mathbf{v} m_k + \mathbf{D}\, \nabla m_k) &= k \cdot m_{k-1} \quad \forall\, k > 0
\end{aligned}
\tag{8}
$$

with the boundary conditions:

$$
\begin{aligned}
\mathbf{n} \cdot \mathbf{v} m_k + \mathbf{n} \cdot (\mathbf{D}\, \nabla m_k) &= 0 \qquad \text{on } \Gamma \setminus \Gamma_2 \\
m_k &= \hat{m}_k \qquad \text{on } \Gamma_2 \\
\mathbf{n} \cdot \mathbf{v} m_k + \mathbf{n} \cdot (\mathbf{D}\, \nabla m_k) &= \mathbf{n} \cdot \mathbf{v} \hat{m}_{k,well} \quad \text{on } \Gamma_{well},\ \forall\, k \geq 0
\end{aligned}
\tag{9}
$$

Here, $\hat{m}_k$ is the k^{th}-raw temporal moment of $\hat{c}$ on the boundaries Γ_2 and Γ_{well}. Because the contaminant release at the well on boundary Γ_{well} is instantaneous at time $t_0 = 0$ and with unit spill concentration, $\hat{m}_{k,well}$ is one for $k = 0$ and zero for all $k \geq 1$. Eq. (8) is formally identical to a steady state partial differential transport equation, which eliminates the need of numerical time integration and directly yields temporal characteristics at very low computational costs.

Using the Maximum Entropy method (e.g., Jaynes [59]) in log-time (e.g., Harvey and Gorelick [38]) to recover the full concentration profile yields for a breakthrough curve at any given location:

$$c(t) = \frac{1}{t} \exp \left(- \sum_{\ell=0}^{n_\ell} \lambda_\ell \cdot \ln t^\ell \right), \tag{10}$$

where $\lambda_\ell = [\lambda_0, \ldots, \lambda_{n_\ell}]$ are Lagrangian parameters which are obtained by solving:

$$m_k = \int_{-\infty}^{+\infty} t^k \cdot \frac{1}{t} \exp \left[- \sum_{\ell=0}^{n_\ell} \lambda_\ell \cdot \ln t^\ell \right] \mathrm{dt}, \tag{11}$$

and n_ℓ is the highest order of moments considered and must be an even number. This non-linear optimization problem Eq. (11) can be solved by the standard Newton method (Mohammad-Djafari [60]). We suggest to evaluate the integral in Eq. (11) by Gauss-Hermite integration (e.g., Abramowitz and Stegun [61]) after transforming to $s = \ln t$.

3.3. Probabilistic well vulnerability criteria

To account for spatial variability and parameter uncertainty, we treat hydraulic conductivity K as a random space function (e.g., Delhomme [62]). K is the most sensitive parameter to assess well-head location (e.g., Feyen et al. [39]). We also allow the geostatistical model to be uncertain within the framework of Bayesian geostatistics (e.g., Kitanidis [63]), by using uncertain mean, trend, covariance parameters and shape (e.g., Nowak et al. [42] and Feyen et al. [39], see Section 3.4). We do so, because uncertain covariances add substantially to the uncertainty of transport (e.g., Riva and Willmann [64]). Further parameters that may be assumed uncertain include recharge q_r and porosity n_e. The latter usually has a smaller influence due to its narrow range in aquifers. Due to the Monte Carlo approach, any other kind of additional uncertainties would be easy to implement, such as uncertain boundary conditions (e.g. Kitanidis [44]), and so forth.

With the equations from Section 3, the four intrinsic well vulnerability criteria from Section 2.2 are calculated for each Monte Carlo realization at all points $\mathbf{x}_i$ in the domain Ω. As a result, we obtain the full probability distributions of the corresponding well vulnerability criteria (here illustrated on the first criterion):

$$P\left(t \geq t_0 \,|\, \mathbf{x} = \mathbf{x}_i\right) = \frac{1}{n_r} \sum_{j=1}^{n_r} I_j(\mathbf{x}_i), \tag{12}$$

with n_r being the total number of Monte Carlo simulations. $I_j(\mathbf{x}_i)$ is an indicator function that assumes a value of unity, if the value t of the respective criterion exceeds the critical value t_0 in realization j at location $\mathbf{x}_i$, and zero else. The results of Eq. (12) may be visualized as maps of vulnerability isopercentiles (VIPs) given a critical value $t_0 = \tau_{crit}$.

3.4. Bayesian geostatistical formulation

Hydraulic conductivity is assumed to be a random space function. Now let $\mathbf{s}$ be a $n_s \times 1$ random space vector $\mathbf{s} = \mathbf{X}\boldsymbol{\beta} + \boldsymbol{\epsilon}_s$ where the mean vector $E[\mathbf{s}] = \mathbf{X}\boldsymbol{\beta}$ represents the trend model, and $\boldsymbol{\epsilon}_s$ denotes zero-mean fluctuations. The distribution of $\mathbf{s}$ follows $\mathbf{s} \sim N\left(\mathbf{X}\boldsymbol{\beta}, \mathbf{C_{ss}}\right)$, i.e. is multi-Gaussian with covariance matrix $\mathbf{C_{ss}}$. Thanks to the flexibility of Monte Carlo simulation and the GLUE as conditioning method (see Section 5.3), arbitrarily complex non-multi-Gaussian models could be employed as well. $\mathbf{X}$ is a $n_s \times p$ matrix with p deterministic trend functions, and $\boldsymbol{\beta}$ is the corresponding $p \times 1$ vector of trend coefficients. For spatially constant mean of $\mathbf{s}$, $\mathbf{X}$ is a $n_s \times 1$ vector with unit entries, and $\boldsymbol{\beta}$ is the actual mean value. In our specific case, the uncertain trend coefficients will follow a normal distribution $\boldsymbol{\beta} \sim N\left(\boldsymbol{\beta}*, \mathbf{C}_{\boldsymbol{\beta\beta}}\right)$ with the expected value vector $\boldsymbol{\beta}*$ and the $p \times p$ covariance matrix $\mathbf{C}_{\boldsymbol{\beta\beta}}$ (e.g., Kitanidis [63]). The distribution of the fluctuations $\boldsymbol{\epsilon}_s$ are defined by the vector of structural parameters $\boldsymbol{\theta}$, containing, for example, variance and scale parameters of the covariance function. Subsequently, $\boldsymbol{\epsilon}_s$ has a covariance matrix $\mathbf{C}_{\mathbf{ss}} = \mathbf{C}(\boldsymbol{\theta})$.

3.5. Uncertainty reduction by conditioning

If catchment-specific data are available from past or current characterization campaigns, it is desirable to condition the probabilistic well vulnerability criteria to a given data set arranged in the $m \times 1$ vector $\mathbf{d}_o$. The data set may comprise direct or indirect data, such as conductivity data from grain size analysis or permeameter tests, drawdown data from well testing, hydraulic tomography or past production data of the drinking water well, temperature or tracer data.

Generally speaking, $\mathbf{d}_o$ is related to $\mathbf{s}$ by some model $\mathbf{d} = \mathbf{f}(\mathbf{s}) + \boldsymbol{\epsilon}_r$. Here, $\mathbf{f}(\mathbf{s})$ is a model that relates observable variables (e.g., conductivity measurements, head observations, well concentrations) to $\mathbf{s}$. The $m \times 1$ measurement error vector $\boldsymbol{\epsilon}_r$ follows an error model, here, with the distribution of $\boldsymbol{\epsilon}_r \sim N(\mathbf{0}, \mathbf{R})$, i.e., with zero mean and $m \times m$ error covariance matrix $\mathbf{R}$, that characterizes the magnitude of measurement error. Then, for known $\mathbf{s}$, the measurements have the distribution $\mathbf{d}|\mathbf{s} \sim N(\mathbf{f}(\mathbf{s}), \mathbf{R})$. According to Bayes theorem, the distribution of $\mathbf{s}$ conditioned on a given data set $\mathbf{d}_o$ and known $\boldsymbol{\beta}$ and $\boldsymbol{\theta}$ is:

$$p(\mathbf{s}|\boldsymbol{\beta}, \boldsymbol{\theta}, \mathbf{d}_o) = \frac{p\left(\mathbf{d}_o|\mathbf{s}\right)\, p\left(\mathbf{s}|\boldsymbol{\beta}, \boldsymbol{\theta}\right)}{p\left(\mathbf{d}_o\right)} \tag{13}$$

The Bayesian distribution (marked by a tilde) for uncertain $\boldsymbol{\beta}$ and $\boldsymbol{\theta}$ is obtained by marginalization (e.g., Kitanidis [63]):

$$\tilde{p}\left(\mathbf{s}|\mathbf{d}_o\right) = \int_{\beta}\int_{\theta} p(\mathbf{s}|\boldsymbol{\beta}, \boldsymbol{\theta}, \mathbf{d}_o)\, p\left(\boldsymbol{\beta}, \boldsymbol{\theta}|\mathbf{d}_o\right) d\boldsymbol{\theta} d\boldsymbol{\beta} \tag{14}$$

In this procedure, the entire joint distribution of $\mathbf{s}, \boldsymbol{\beta}$ and $\boldsymbol{\theta}$ is jointly conditioned on $\mathbf{d}_o$ (e.g., Woodbury and Ulrych [65], Pardo-Iguzquiza [66]). Using the Bayesian GLUE (e.g., Feyen et al. [39]), conditioning the probabilistic well vulnerability criteria is achieved by

$$\widetilde{p}(t \geq t_0 \,|\, \mathbf{x}_i,\, \mathbf{d}_o) = \frac{1}{n_r} \cdot \sum_{j=1}^{n_r} w_j \cdot I_j \tag{15}$$

with the weights $w_j = \frac{L_j}{\sum_{j=1}^{n} L_j}$, representing the likelihood L of realization j given $\mathbf{d}_o$:

$$L\left(\mathbf{s}_j, \boldsymbol{\theta}_j, \boldsymbol{\beta}_j|\mathbf{d}_o\right)_j = \left(\frac{1}{2\pi \cdot ||\mathbf{R}||}\right)^{m/2} \exp\left[-\frac{1}{2}\left(\mathbf{d}_o - \mathbf{d}_{sim}(\mathbf{s}_j)\right)^T \mathbf{R}^{-1} \left(\mathbf{d}_o - \mathbf{d}_{sim}(\mathbf{s}_j)\right)\right],$$

where $\mathbf{d}_{sim}(\mathbf{s}_j) = \mathbf{f}(\mathbf{s})$ is the corresponding simulated data set of realization j.

For reasons of computational efficiency, it is beneficial to process direct point-scale measurements of parameters with extremely fast kriging-like conditional simulation techniques (e.g., Fritz et al. [67]) in combination with conditional sampling to represent the weights w_j of covariance parameters (e.g., Pardo-Iguzquiza [66]). The uncertain mean and trend coefficients may be directly included in the kriging procedure (e.g., Kitanidis [63] and Fritz et al. [67]). By applying rejection sampling (proportional to L_j) in the conditioning of $\boldsymbol{\theta}$ on direct data and of $\mathbf{s}$, $\boldsymbol{\beta}$, $\boldsymbol{\theta}$ on indirect data, all considered realizations are finally equally likely.

4. Illustrative Example

4.1. Model Set up

We illustrate the methodology on a rectangular 2D example with domain size $300m \times 300m$ (see Fig. 3). This example only serves for illustrative purposes, as the method is independent of dimensionality, complex geometries and boundary conditions. A hydraulic background gradient from west to east with $\nabla\phi = 0.005$ is assumed with appropriate fixed head conditions on all boundaries. Within the reverse approach, a Dirac-pulse with concentration $\hat{c}_{spill}$ is introduced at a single well at $x = 225m$ and $y = 150m$ with a pumping rate of $Q = 1 \times 10e^{-4} m^3 s^{-1}$. The aquifer is assumed to be leaky confined with an uncertain normally distributed and spatially constant recharge rate of $q_{rg} = 120mm\,a^{-1}$ and standard deviation $\sigma_{rg} = 10mm\,a^{-1}$.

The discretization of the domain equals $dx = dy = 1m$ with assumed subgrid-scale dispersivities of $\alpha_L = 2.5m$ and $\alpha_T = 0.25m$. The total number of nodes to solve are $n_{tot} = 96.301$. As covariance model for log-transmissivity $Y = \ln(T)$, we choose the Matérn correlation function (e.g., Handcock and Stein [68]) because it has an additional shape parameter κ. Treating κ as uncertain resembles Bayesian model averaging over a continuous spectrum of covariance shapes (e.g., Nowak et al. [42]). The parameters of the structural model are $\boldsymbol{\theta} = (\mu, \sigma^2, \kappa, \lambda_x, \lambda_y)$, where μ is the mean value of log-transmissivity $Y = ln(T)$ (with T in units of $m^2 s^{-1}$) , σ^2 is the variance, κ is the shape parameter, and λ_x, λ_y are the length scales. At the prior stage, we assume them to follow uniform distributions with lower and upper bounds, $\mu = [-7.5 \;\; -5.5]$, $\sigma^2 = [1 \;\; 3]$, $\kappa = [0.5 \;\; 5]$, $\lambda_x = [10 \;\; 25]\,m$ and $\lambda_y = [5 \;\; 15]\,m$.

Unconditional transmissivity fields are generated and flow and transport simulations are performed with the same numerical implementation as in Nowak et al. [69]. The simulations were run on a dual core processor @2.8GHz with 4GB Ram. The computational time for $n = 500$ unconditional realizations is $22h$ and, in the conditional case, $24h$. In order to demonstrate the impact of data through conditioning, we generate a "synthetic truth" random realization. From this we draw five artificial measurements of head ϕ_o and ten measurements of log-transmissivity Y (see Fig. 3), perturbed with random measurement error that has standard deviation of $\sigma_Y = 1$ and $\sigma_\phi = 0.25m$, respectively. The structural parameters used to generate the synthetic random field are $\mu_o = -6.83$, $\sigma_o^2 = 1.91$, $\kappa_o = 0.49$, $\lambda_{x,o} = 9.11\,m$ and $\lambda_{y,o} = 5.17\,m$. For conditional simulation, we use the methods discussed in Section 3.5.

4.2. Unconditional Results

Fig. 4 displays the four intrinsic well vulnerability criteria with isopercentiles of [0.1, 0.5, 0.9], based on the illustrative example for unconditional realizations. Fig 4 (a) represents the German well-head protection area with $\tau_{crit} = 50d$ [54], but here evaluated for the arrival time of peak concentration instead of bulk arrival time. The second vulnerability criterion is given in Fig. 4 (b), showing the area within which a contamination is being diluted by less than a factor of $\zeta_{crit} = 1 \times 10^{-7}$. Fig. 4 (c) shows the probabilistic extent of the capture zone, in which a critical reaction time $\tau_{crit} = 50d$ is exceeded, thus indicating the confidence in the reaction time for a water manager until the contamination breaches the given threshold level $\chi_{crit} = 1 \times 10^{-7}$. The fourth criterion is shown in Fig. 4 (d), indicating the potential area for spills where the well is exposed to contamination above the threshold for more than $\tau_{exp} = 2d$. The choice of the critical levels for the second to fourth well vulnerability criteria substantially influence shape and size of the corresponding vulnerability maps. If the critical peak level ζ_{crit} for the second vulnerability criterion (see (b) in Fig. 4), Fig. 5 and Fig. 6) equals the threshold level χ_{crit} for the third and fourth vulnerability criterion (see (c) and (d) in Fig. 4), Fig. 5 and Fig. 6), the isopercentiles of the reaction time can be at most as wide as the isopercentiles of peak level. For large critical values of reaction time τ_{crit} and $\zeta_{crit} = \chi_{crit}$, the isopercentiles of the third well vulnerability criterion becomes equal to the isopercentiles of the second criterion, because the third criterion will degenerate to the information that *any* reaction time is necessary. The same effect occurs for the fourth vulnerability criterion for small values of the critical exposure levels τ_{exp}, because non-zero exposure times appear where-ever the critical threshold level χ_{crit} is breached.

4.3. Conditional Results

The actual outlines for the critical values that apply in the synthetic "real" realization are shown in Fig. 5. For comparison purposes, we will discuss location A, marked with a plus sign. Location A has peak arrival time $t_{peak,obs} = 68d$, dilution of peak concentration by the factor of $c_{peak,obs} = 1.04 \times 10^{-7}$, time to react $t_{crit,obs} = 64d$ and exposure time $t_{exp,obs} = 8d$. Fig. 6 shows the corresponding results for the conditional Monte Carlo simulations using the synthetic data set, obtained from the synthetic truth shown in Fig. 5.

5. Discussion

5.1. VIP maps

For any risk assessment study it is important to determine both the exposure level to the hazardous contamination and the likelihood of its occurrence. Considering the two given examples (unconditional and conditional realizations), both risk-based information types are contained within the VIP maps, showing for each location the existing intrinsic well vulnerability of the drinking water well and its exceedance probability. The ensemble-averaged vulnerability criteria plotted in the background of Fig. 4, Fig. 5 and Fig. 6 are, per definition, equivalent to solutions based on macrodispersion approaches. Therefore, their spatial distribution and features are discussed in Frind et al. [1]. For discussion of the new probabilistic context, let us assume a spill event (i.e. virologically or microbially loaded water) at location A, marked in Fig. 4, Fig. 5 and Fig. 6 by a plus sign.

The ensemble average peak arrival time from A to the well is estimated (ensemble mean) for the unconditional case with $t_{A,uncond} = 57d$ (see Fig. 4(a)) and for the conditioned example $t_{A,cond} = 76d$ (see Fig. (a)). In a conventional approach, the stakeholder would assume that there will be no exposure risk for the drinking water well by the spill event at A in both cases, as microbial safety is defined in Germany by transport times larger than $\tau_{crit} = 50d$. Taking the new probabilistic information into account, the vulnerability maps for peak arrival show exceedance probabilities $\widetilde{P}(t > \tau_{crit})_{A,uncond} = 59.5\%$ and $\widetilde{P}(t > \tau_{crit})_{A,cond} = 28.5\%$. This is indeed a substantial risk, and would be invisible within conventional deterministic approaches. The actual choice of the delineated area will depend on the desired confidence level of the stakeholders (see Section 5.3).

The second well vulnerability criterion directly shows the relevance of distinguishing between dilution and the uncertainty of plume location. The expected maximum concentration at the well is, on average, diluted by the factor of $c_{peak,uncond} = 1.25 \times 10^{-7}$ and $c_{peak,cond} = 9.68 \times 10^{-8}$ until it reaches the well, if a contamination occurred at location A. Single realizations can yield higher and lower dilution factors, as shown in Fig. 7. In a macrodispersion approach, one would directly obtain the ensemble-averaged breakthrough curve. The statistical information of what peak concentrations occur with what probability would not be accessible. Much worse, the average over strongly peaked distributions with peaks at different peak arrival times leads to a much smaller peak level of the macrodispersive (implicitly ensemble averaged) breakthrough curves (see Fig. 7). This illustrates best, why macrodispersive approaches are not adequate for probabilistic risk assessment, if transport is non-ergodic (e.g. Hassan et al. [70]). Not just arrival time of the peak or bulk is primarily of interest for catchment managers (see Section 5.2), but also the time until a given threshold value in the well is breached after a spill within the catchment. By taking the third vulnerability criterion into account, water managers can know the time to react before the well has to be shut down. In our example, the average values for location A are $t_{crit,uncond} = 28d$ and $t_{crit,cond} = 44d$, which is substantially smaller than the numbers for peak arrival time. All realizations, which do not breach the threshold level $\chi_{crit} = 1 \times 10^{-7}$, are not considered within the ensemble averaging as no reaction time is required at all. The $10^{\text{th}}-$ percentile of available reaction time at location A is as low as $12d$ (uncond) and $22d$ (cond), indicating how fast early alert systems and emergency management decisions would have to be, such that well safety can still be guaranteed in adverse cases.

Finally, the fourth vulnerability criterion gives the necessary information about the well down time to be expected after contamination by a spill event within the catchment. The average exposure time related to a spill at location A is $t_{exp,uncond} = 7d$ and $t_{exp,cond} = 7d$, showing exceedance probability of $\widetilde{P}(t > \tau_{exp})_{A,uncond} = 45.8\%$ and $\widetilde{P}(t > \tau_{exp})_{A,uncond} = 37.4\%$. This indicates the time frame and the associated uncertainty that the well will be out of operation. If desired, even histograms about the exposure time to spills at location A could be plotted. Together, the third (time to react) and the fourth vulnerability criterion (well down time) provide the necessary information for financial optimization of risk treatment alternatives, while criteria one and two yield the essential information for toxicity assessment in human health risk assessment.

5.2. Peak versus bulk arrival time

The typically positively skewed breakthrough curves of transport in heterogeneous formations yield earlier arrival time for peak concentrations t_{peak} than for the arrival of bulk mass t_{50} at the well [71]. Fig. 9 illustrates this with a scatter plot between t_{peak} and t_{50}. In our example, $t_{peak,uncond}$ ($t_{peak,cond}$) is on average 17% (13%) smaller than t_{50}, leading to 7% (5%) larger catchment delineation on average, as shown in Fig. 8. The size difference depends on the degree of heterogeneity, and will be more drastic for high variability cases or fractured media. In risk analysis, the underestimation of protection zones when using bulk arrival time can have crucial liability issues in risk-based decisions. The advantage of our first vulnerability criterion over the traditional bulk-related assessment is that it takes the more conservative peak time instead of the bulk arrival time into account, which we deem the more relevant aspect of contaminant arrival in this context.

5.3. Area enclosed by the VIP lines and the effect of conditioning

The uncertainty in actual location of A_{crit} can easily overwhelm the uncertainty in its size, leading to much larger well-head delineation under uncertainty. The actual choice of the delineated area will depend on the desired confidence level of the stakeholders, i.e., which isopercentile to choose for delineation. A possible measure for the effect of uncertainty on the areal demand of delineation is the area between the $10^{th}-$ and $90^{th}-$percentile contours of the well vulnerability criteria, normalized by the area within the $50^{th}-$percentile contour:

$$U = \frac{A_{90} - A_{10}}{A_{50}} \tag{16}$$

U is a measure for the area a planner has to sacrifice due to uncertainty. The corresponding unconditional and conditional values of U for all four vulnerability criteria in our illustrative example are provided in Table 1.

Conditioning reduces the uncertainty and leads to vulnerability maps with larger information content, moving closer to reality. The distances between the single isopercentiles decline, leading to a more distinct delineation of the well-head protection area. Clearly, it is worth to spend money on site investigation because it reduces the areal demand of uncertainty (compare Feyen et al. [39]). For example, conditioning on ten transmissivity and five head measurements has the areal demand of uncertainty U by 17.9% in our example for the well-head protection area based on VIP one.

VIP	"critical value"	unconditional uncertainty U_{uc}	conditional uncertainty U_c
t_{peak}	$\tau_{crit} = 50d$	43.1%	25.2%
c_{peak}	$\zeta_{crit} = 1 \times 10^{-7}[-]$	14.6%	10.4%
t_{crit}	$\tau_{crit} = 50d$	14.6%	10.4%
t_{exp}	$\tau_{exp} = 2d$	14.5%	10.3%

Table 1: Showing the fractional area [%] of delineated catchments according to the four VIP maps that is sacrificed to uncertainty for the conditioned and the unconditioned case.

In comparison to macrodispersive approaches, i.e., without separation of dilution and uncertainty in position, no VIP maps, but only one line could be shown (e.g., Frind et al. [1]). In that case, uncertainty in size and position is lumped together within an implicitly averaged transport equation, blurring the overall picture.

The quantity and quality of data required to reduce the uncertainty within a probabilistic assessment process to an acceptable level can be determined in a rational manner when considering the worth of data through optimal design techniques (e.g., Nowak et al. [42], Feyen et al. [39]). Such techniques can also answer the question, which types of data should be collected where, in order to achieve the largest reduction of sacrificed area for a given limited investigation budget. Overall, the economic benefit of more confident and yet smaller delineation could thus be optimized versus the costs of data collection and alternative risk management options such as remediation, enhanced water treatment and so forth.

6. Summary and Conclusions

In this paper, we cast the four intrinsic well vulnerability criteria by Frind et al. [1] into a probabilistic framework. For illustration and discussion, we applied them to a synthetic example with a 2D semi-confined heterogeneous aquifer with a single pumping well. Via Monte Carlo simulation, we calculate maps of vulnerability isopercentiles (VIP maps), showing the probability that a given critical level of vulnerability is exceeded anywhere in the domain. To discuss the impact of conditioning on data, we used a synthetic data set with head and transmissivity values, and compared conditional and unconditional VIP maps.

As the four vulnerability criteria are sensitive to the conceptual difference between uncertainty in plume location and actual dilution, we solved the flow and transport problem via finely resolved Monte Carlo simulations, where we resolve aquifer heterogeneity on and above the grid-scale in each realization. Therefore, the probability of peak concentration levels and the uncertainty in position and extent of protection zones can be assessed separately. Compared to purely advective or non-probabilistic approaches, our concept provides valuable additional probabilistic and advective-dispersive information, such as

1. The probability distribution of peak arrival travel time from a potential spill location to the well;
2. The possible levels of peak concentration arriving at the well, while accounting for dilution effects through diffusion and dispersion;
3. The probability distribution of the time window available to react after a spill event until a critical concentration level is exceeded in the well

(e.g., a drinking water standard); and

4. The probability that the well has to be shut down for more than a given duration, which is the information required to estimate economical damage and consider alternative risk treatment measures.

Our vulnerability isopercentile maps are easy to understand, such as showing the level of exposure risk for all locations within the well catchment. By visualizing zones of higher and lower vulnerability probabilities, they allow to prioritize remediation of contaminated sites and location of protection zones. Although our approach uses Monte Carlo to resolve heterogeneity even at small scales, the computational costs are kept moderate by combining the reverse formulation of advective-dispersive transport and the concept of temporal moments. Despite the (small) loss of information due to the temporal moment approach, the gain in computational efficiency and the resulting accessibility of probabilistic information are more valuable in our opinion.

The suggested approach can account for arbitrary sources of uncertainty, and is independent of the chosen geostatistical conditioning scheme. It can be used as an add-on to almost any commercial software, because it does not require intrusion into the code. Furthermore, the concept is independent of dimensionality, boundary conditions and employed simulation software. These properties make the approach flexible for any type of drinking water catchments and a wide range of applications.

When this approach is coupled with specific toxicity parameters for individual groups of contaminants, human health risk assessment can be performed as a last step in probabilistic risk assessment over all risk scales. The given exposure time and level is then depending not only on the intrinsic aquifer behavior, but also on the studied exposure route defined by the reference concentration (RfC) or reference dose (RfD) (e.g., US EPA [3], Cushman et al. [32]). The resulting exposure profile with its exposure duration gives a precise and more reliable input variable for human health risk assessment, as all information on amount, duration and frequency with its associated uncertainties are available.

In conclusion, our VIP maps display probabilistic information in a way that is easy to understand. We believe that our concept provides all the fundamental basis for probabilistic risk assessment in actively managed well catchments, and can provide stakeholders with the necessary information and tools to develop complete risk management schemes as recommended by the Water Safety Plans.

In addition, to further reduce the uncertainty towards better risk management, a combination with optimal design of investigation strategies is straightforward. Even an overall rational optimization between the areal demand of delineation, costs for data acquisition and alternative risk treatment methods is possible.

Acknowledgments. This study has been funded in parts by the Cluster of Excellence in Simulation Technology (EXC 310/1) at the University of Stuttgart. The author is indebted to Felipe de Barros, Philip Binning and Martin Emmert for their productive discussions to the manuscript.

References

[1] E. Frind, J. Molson, D. Rudolph, Well vulnerability: A quantitative approach for source water protection, Ground Water 44 (5) (2006) 732–742.

[2] US NRC, Reactor safety study - an assessment of accident risks in US commercial nuclear power plants, US Nuclear Regulatory Commission, Washington, DC, 1975.

[3] US EPA, Risk Assessment Guidance for Superfund Volume I: Human Health Evaluation Manual (Part A), EPA/540/1-89/002 edn., 1989.

[4] WHO, Guidelines for Drinking-Water Quality, 2004.

[5] A. Davison, G. Howard, M. Stevens, P. Callan, D. Deere, J. Bartram, Water safety plans - Managing drinking-water quality from catchment to consumer, Geneva, Switzerland: World Health Organization (WHO/SDE/WSH/05.06).

[6] European Council Directive Council Directive 98/83/EC, The quality of water intended for human consumption, The Council of the European Union, 1998.

[7] US EPA, Guidelines for delineation of wellhead protection areas, EPA - 440/5-93-001 edn., 1993.

[8] S. Evers, D. Lerner, How uncertain is our estimate of a wellhead protection zone?, Ground Water 36 (1) (1998) 49–57, ISSN 0017-467X.

[9] S. Neuman, Maximum likelihood Bayesian averaging of uncertain model predictions, Stochastic Environmental Research and Risk Assessment 17 (5) (2003) 291–305.

[10] J. A. Hoeting, R. A. Davis, A. A. Merton, S. E. Thompson, Model Selection for Geostatistical Models, Ecological Applications 16 (1) (2006) 87–98, ISSN 10510761.

[11] I. Park, H. Amarchinta, R. Grandhi, A Bayesian approach for quantification of model uncertainty, Reliability Engineering & System Safety 95 (7) (2010) 777–785.

[12] Y. Rubin, Applied stochastic hydrogeology, Oxford University Press, USA, 2003.

[13] T. Aven, Some reflections on uncertainty analysis and management, Reliability Engineering & System Safety 95 (3) (2010) 195–201, ISSN 0951-8320, doi:10.1016/j.ress.2009.09.010.

[14] L. Feyen, K. Beven, F. De Smedt, J. Freer, Stochastic capture zone delineation within the generalized likelihood uncertainty estimation methodology: Conditioning on head observations, Water Resources Research 37 (3) (2001) 625–638, ISSN 0043-1397.

[15] M. Varljen, J. Shafer, Assessment of uncertainty in time-related capture zone using conditional simulation of hydraulic conductivity, Ground Water 29 (5) (1991) 737–748.

[16] S. Franzetti, A. Guadagnini, Probabilistic estimation of well catchments

in heterogeneous aquifers, Journal of Hydrology 174 (1-2) (1996) 149–171.

[17] M. van Leeuwen, C. te Stroet, A. Butler, J. Tompkins, Stochastic determination of well capture zones, Water Resources Research 34 (9) (1998) 2215–2223, ISSN 0043-1397.

[18] E. Jacobson, R. Andricevic, J. Morrice, Probabilistic capture zone delineation based on an analytic solution, Ground Water 40 (1) (2002) 85–95.

[19] F. Stauffer, H. Franssen, W. Kinzelbach, Semianalytical uncertainty estimation of well catchments: Conditioning by head and transmissivity data, Water Resources Research 40 (8) (2004) W08305, doi: 10.1029/2004WR003320.

[20] S. Vassolo, W. Kinzelbach, W. Schafer, Determination of a well head protection zone by stochastic inverse modelling, Journal of Hydrology 206 (3-4) (1998) 268–280, ISSN 0022-1694.

[21] K. Moutsopoulos, A. Gemitzi, V. Tsihrintzis, Delineation of groundwater protection zones by the backward particle tracking method: theoretical background and GIS-based stochastic analysis, Environmental Geology 54 (5) (2008) 1081–1090, ISSN 0943-0105, doi:10.1007/s00254-007-0879-3.

[22] B. Cole, S. Silliman, Utility of simple models for capture zone delineation in heterogeneous unconfined aquifers, Ground Water 38 (5) (2000) 665–672, ISSN 0017-467X.

[23] A. Guadagnini, S. Franzetti, Time-related capture zones for contaminants in randomly heterogeneous formations, Ground Water 37 (2) (1999) 253–260.

[24] D. Pollock, Semianalytical computation of path lines for finite-difference models., Ground Water 26 (6) (1988) 743–750.

[25] T. Tosco, R. Sethi, A. Di Molfetta, An automatic, stagnation point based algorithm for the delineation of Wellhead Protection Areas, Water Resources Research 44 (7) (2008) W07419, ISSN 0043-1397, doi: 10.1029/2007WR006508.

[26] L. Gelhar, C. Axness, Three-dimensional stochastic analysis of macrodispersion in aquifers, Water Resources Research 19 (1) (1983) 161–180.

[27] G. Dagan, Solute transport in heterogeneous porous formations, Journal of Fluid Mechanics 145 (1984) 151–177.

[28] R. Andricevic, V. Cvetkovic, Relative dispersion for solute flux in aquifers, Journal of Fluid Mechanics 361 (1998) 145–174.

[29] M. Dentz, H. Kinzelbach, S. Attinger, W. Kinzelbach, Temporal behavior of a solute cloud in a heterogeneous porous medium 1. Point-like injection, Water Resources Research 36 (12) (2000) 3591– 3604.

[30] P. Kitanidis, The concept of the dilution index, Water Resources Research 30 (7) (1994) 2011–2026.

[31] T. Oberg, B. Bergback, A review of probabilistic risk assessment of

contaminated land, Journal of Soils and Sediments 5 (4) (2005) 213–224, ISSN 1439-0108, doi:10.1065/jss2005.08.143.

[32] D. Cushman, K. Driver, S. Ball, Risk assessment for environmental contamination: an overview of the fundamentals and application of risk assessment at contaminated sites, Canadian Journal of Civil Engineering 28 (2001) 155–162.

[33] F. P. J. de Barros, Y. Rubin, A Risk-Driven Approach for Subsurface Site Characterization, Water Resources Research 44 (2008) W01414, doi:10.1029/2007WR006081.

[34] F. P. J. de Barros, Y. Rubin, R. Maxwell, The concept of comparative information yield curves and its application to risk-based site characterization, Water Resources Research 45 (6) (2009) W06401, doi: 10.1029/2008WR007324.

[35] F. P. J. de Barros, D. Bolster, X. Sanchez-Vila, W. Nowak, A Divide and Conquer Approach to Cope with Uncertainty, Human Health Risk and Decision Making in Contaminant Hydrology, Water Resources Research (2010) SUBMITTED.

[36] O. Cirpka, A. Valocchi, Two-dimensional concentration distribution for mixing-controlled bioreactive transport in steady state, Advances in Water Resources 30 (6-7) (2007) 1668–1679.

[37] R. Neupauer, J. Wilson, Adjoint-derived location and travel time probabilities for a multidimensional groundwater system, Water Resources Research 37 (6) (2001) 1657–1668.

[38] C. Harvey, S. Gorelick, Temporal moment-generating equations - Modeling transport and mass-transfer in heterogeneous aquifers, Water Resources Research 31 (8) (1995) 1895–1911, ISSN 0043-1397.

[39] L. Feyen, P. Ribeiro, J. Gomez-Hernandez, K. Beven, F. De Smedt, Bayesian methodology for stochastic capture zone delineation incorporating transmissivity measurements and hydraulic head observations, Journal of Hydrology 271 (1-4) (2003) 156–170, ISSN 0022-1694.

[40] US EPA, Guiding Principles for Monte Carlo Analysis, Washington, D.C., epa/630/r-97/001 edn., 1997.

[41] L. Feyen, P. Ribeiro, F. De Smedt, P. Diggle, Bayesian methodology to stochastic capture zone determination: Conditioning on transmissivity measurements, Water Resources Research 38 (9) (2002) 1164, ISSN 0043-1397, doi:10.1029/2001WR000950.

[42] W. Nowak, F. de Barros, Y. Rubin, Bayesian geostatistical design: Task-driven optimal site investigation when the geostatistical model is uncertain, Water Resources Research 46 (3) (2010) W03535, doi: 10.1029/2009WR008312.

[43] A. Zanini, P. Kitanidis, Geostatistical inversing for large-contrast transmissivity fields, Stochastic Environmental Research and Risk Assessment 23 (5) (2009) 565–577.

[44] P. Kitanidis, Quasi-linear geostatistical theory for inversing, Water Resources Research 31 (10) (1995) 2411–2419.

[45] W. Nowak, O. Cirpka, A modified Levenberg-Marquardt algorithm for quasi-linear geostatistical inversing, Advances in Water Resources 27 (7) (2004) 737–750.

[46] A. Alcolea, J. Carrera, A. Medina, Pilot points method incorporating prior information for solving the groundwater flow inverse problem, Advances in Water Resources 29 (11) (2006) 1678–1689.

[47] H. Franssen, J. Gómez-Hernández, A. Sahuquillo, Coupled inverse modelling of groundwater flow and mass transport and the worth of concentration data, Journal of Hydrology 281 (4) (2003) 281–295.

[48] H. Franssen, A. Alcolea, M. Riva, M. Bakr, N. van der Wiel, F. Stauffer, A. Guadagnini, A comparison of seven methods for the inverse modelling of groundwater flow. Application to the characterisation of well catchments, Advances in Water Resources 32 (6) (2009) 851–872.

[49] G. Uffink, Application of Kolmogorov backward equation in random walk simulations of groundwater contaminant transport, in: H. E. Kobus, W. Kinzelbach (Eds.), Contaminant Transport in Groundwater: Proceedings of the International Symposium on Contaminant Transport in Groundwater, A. A. Balkema, Brookfield, Vt., 283–298, 1989.

[50] O. Cirpka, P. Kitanidis, Characterization of mixing and dilution in heterogeneous aquifers by means of local temporal moments, Water Resources Research 36 (5) (2000) 1221–1236, ISSN 0043-1397.

[51] T. Reilly, D. Pollock, Sources of water to wells for transient cyclic systems, Ground Water 34 (6) (1996) 979–988, ISSN 0017-467X.

[52] E. Jaynes, Information theory and statistical mechanics, Physical Review 106 (4) (1957) 620–630, ISSN 0031-899X.

[53] A. Woodbury, T. Ulrych, Minimum relative entropy and probabilistic inversion in groundwater hydrology, Stochastic Hydrology and Hydraulics 12 (5) (1998) 317–358, ISSN 0931-1955.

[54] DVGW, Arbeitsblatt W101: Richtlinien fuer Trinkwasserschutzgebiete; Teil 1: Schutzgebiete fuer Grundwasser, 2006.

[55] ISO/IEC: 31010, Risk management - Risk assessment techniques, International Electrotechnical Commission, IEC, 2009.

[56] A. Scheidegger, General Theory of Dispersion in Porous Media, Journal of Geophysical Research 66 (10) (1961) 3273, ISSN 0148-0227.

[57] R. Neupauer, J. Wilson, Adjoint method for obtaining backward-in-time location and travel time probabilities of a conservative groundwater contaminant, Water Resources Research 35 (11) (1999) 3389–3398, ISSN 0043-1397.

[58] D. Wackerly, W. Mendenhall, R. Scheaffer, Mathematical statistics with applications, vol. ISBN: 0495110817 / ISBN-13: 9780495110811, Duxbury Press, 7 edn., 2002.

[59] E. Jaynes, Probability theory: the logic of science, Cambridge Univ Press, 2003.

[60] A. Mohammad-Djafari, A Matlab Program to Calculate the Maximum Entropy Distributions, in: C. Smith, G. Erickson, P. Neudorfer (Eds.),

Maximum Entropy and Bayesian Methods, vol. 50 of *Fundamental Theories of Physics*, Eleventh International Workshop on Maximum Entropy and Bayesian Methods of Statistical Analysis, Kluwer Academic Publishers, 221–234, doi:2001physics.11126M, 2001.

[61] M. Abramowitz, I. Stegun, Handbook of mathematical functions with formulas, graphs, and mathematical tables, Dover publications, chapter 25.4 Gaussian Quadrature, 1964.

[62] J. Delhomme, Spatial variability and uncertainty in groundwater-flow parameters - Geostatistical approach, Water Resources Research 15 (2) (1979) 269–280, ISSN 0043-1397.

[63] P. Kitanidis, Parameter uncertainty in estimation of spatial functions: Bayesian analysis, Water Resources Research 22 (4) (1986) 499–507.

[64] M. Riva, M. Willmann, Impact of log-transmissivity variogram structure on groundwater flow and transport predictions, Advances in Water Resources 32 (8) (2009) 1311–1322, ISSN 0309-1708.

[65] A. Woodbury, T. Ulrych, A full-Bayesian approach to the groundwater inverse problem for steady state flow, Water resources research 36 (8) (2000) 2081–2093.

[66] E. Pardo-Iguzquiza, Bayesian inference of spatial covariance parameters, Mathematical Geology 31 (1) (1999) 47–65.

[67] J. Fritz, I. Neuweiler, W. Nowak, Application of FFT-based algorithms for large-scale universal kriging problems, Mathematical Geosciences 41 (5) (2009) 509–533.

[68] M. Handcock, M. Stein, A Bayesian analysis of kriging, Technometrics 35 (4) (1993) 403–410.

[69] W. Nowak, R. Schwede, O. Cirpka, I. Neuweiler, Probability density functions of hydraulic head and velocity in three-dimensional heterogeneous porous media, Water Resources Research 44 (2008) W08452, doi:10.1029/2007WR006383.

[70] A. Hassan, R. Andricevic, V. Cvetkovic, Evaluation of analytical solute discharge moments using numerical modeling in absolute and relative dispersion frameworks, Water Resources Research 38 (2) (2002) W1009.

[71] R. Haggerty, S. Gorelick, Multiple-rate mass transfer for modeling diffusion and surface reactions in media with pore-scale heterogeneity, Water Resources Research 31 (10) (1995) 2383–2400.

Figure 1: Methodology to determine probabilistic intrinsic well vulnerability criteria

Figure 2: Illustrative sketch showing the four intrinsic well vulnerability criteria and temporal moments characterizing the concentration breakthrough curve $c(t)$

Figure 3: Illustrative Example, showing location of measurements

Figure 4: Probabilistic isopercentiles $[0.1, 0.5, 0.9]$ for the four intrinsic well vulnerability criteria (a)-(d) from $n = 500$ unconditioned simulations. Grey-scale maps show the ensemble mean of the respective well vulnerability criteria (a)-(d)

Figure 5: Outlines and criteria values of the "real" realization

Figure 6: Probabilistic isopercentiles $[0.1, 0.5, 0.9]$ for the four intrinsic well vulnerability criteria (a)-(d) from $n = 500$ conditioned simulations. Grey-scale maps show the ensemble mean of the respective well vulnerability criteria

Figure 7: Breakthrough curves (BTC) of all realizations and the average breakthrough curve (bold) of $n = 500$ unconditional realizations at the drinking water well, if a hazardous spill occurred at location A

Figure 8: Showing the size of the time-related well-head protection zones, depending on t_{peak} and t_{50} for different isopercentile levels in the unconditional (left) and conditional (right) case

Figure 9: Scatter plot of mean peak arrival t_{peak} versus mean bulk arrival time t_{50}

Figure 1
Click here to download Figure: run_ablauf_awr.eps

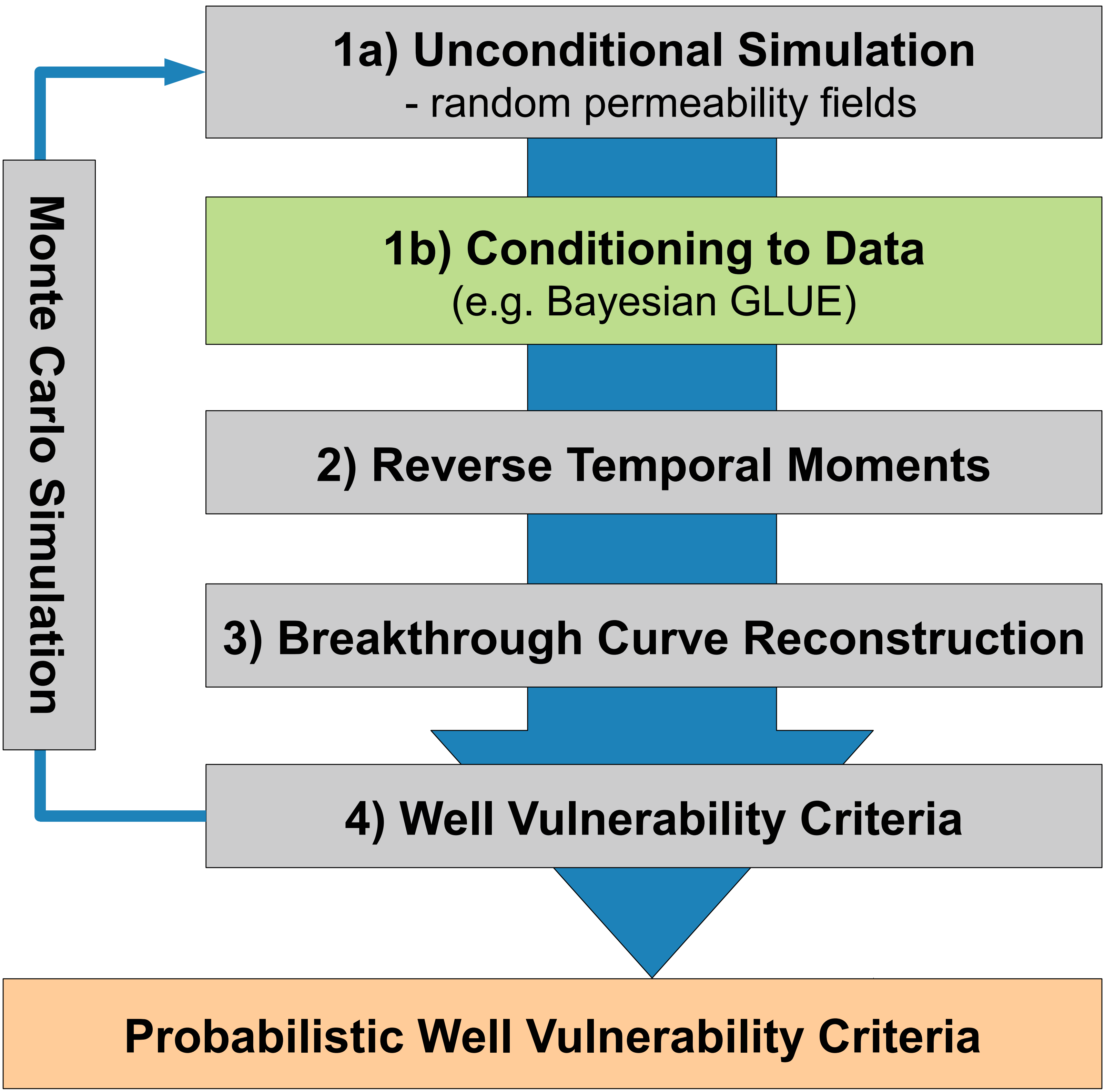

Figure 2
Click here to download Figure: btc_moments.eps

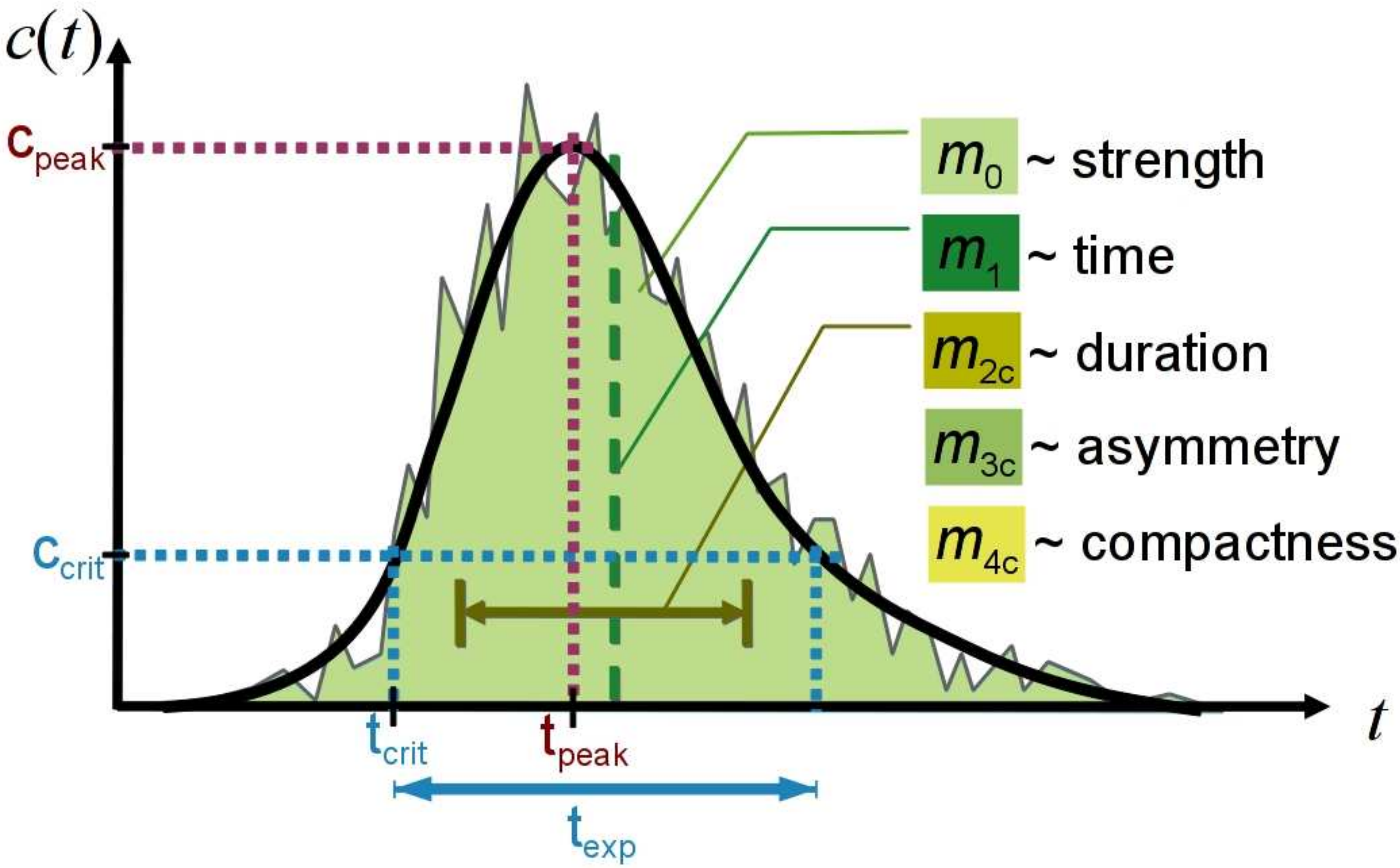

Figure 3
Click here to download Figure: fig3_illus_ex.eps

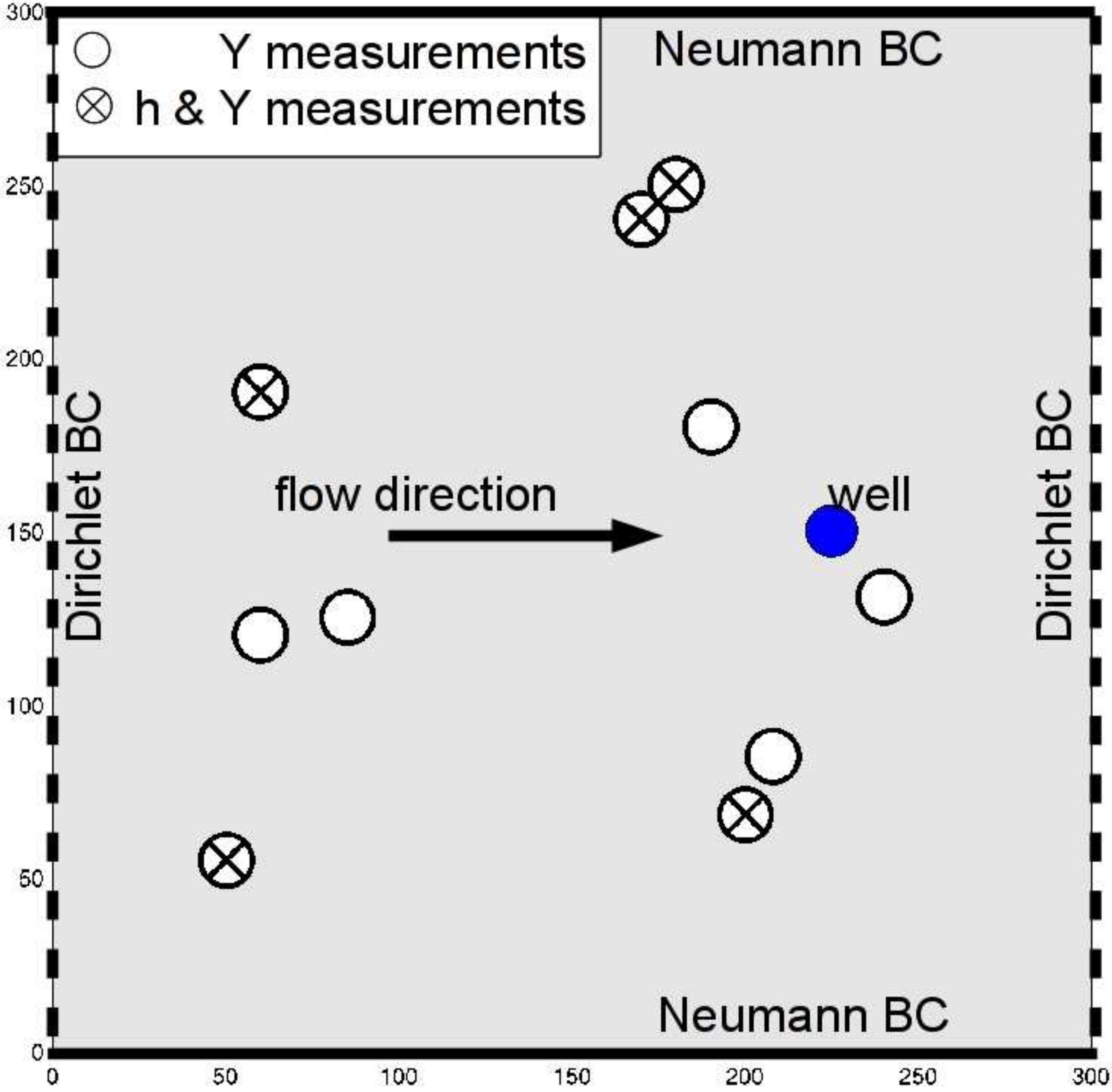

Figure 4
Click here to download Figure: Fig4uncond.eps

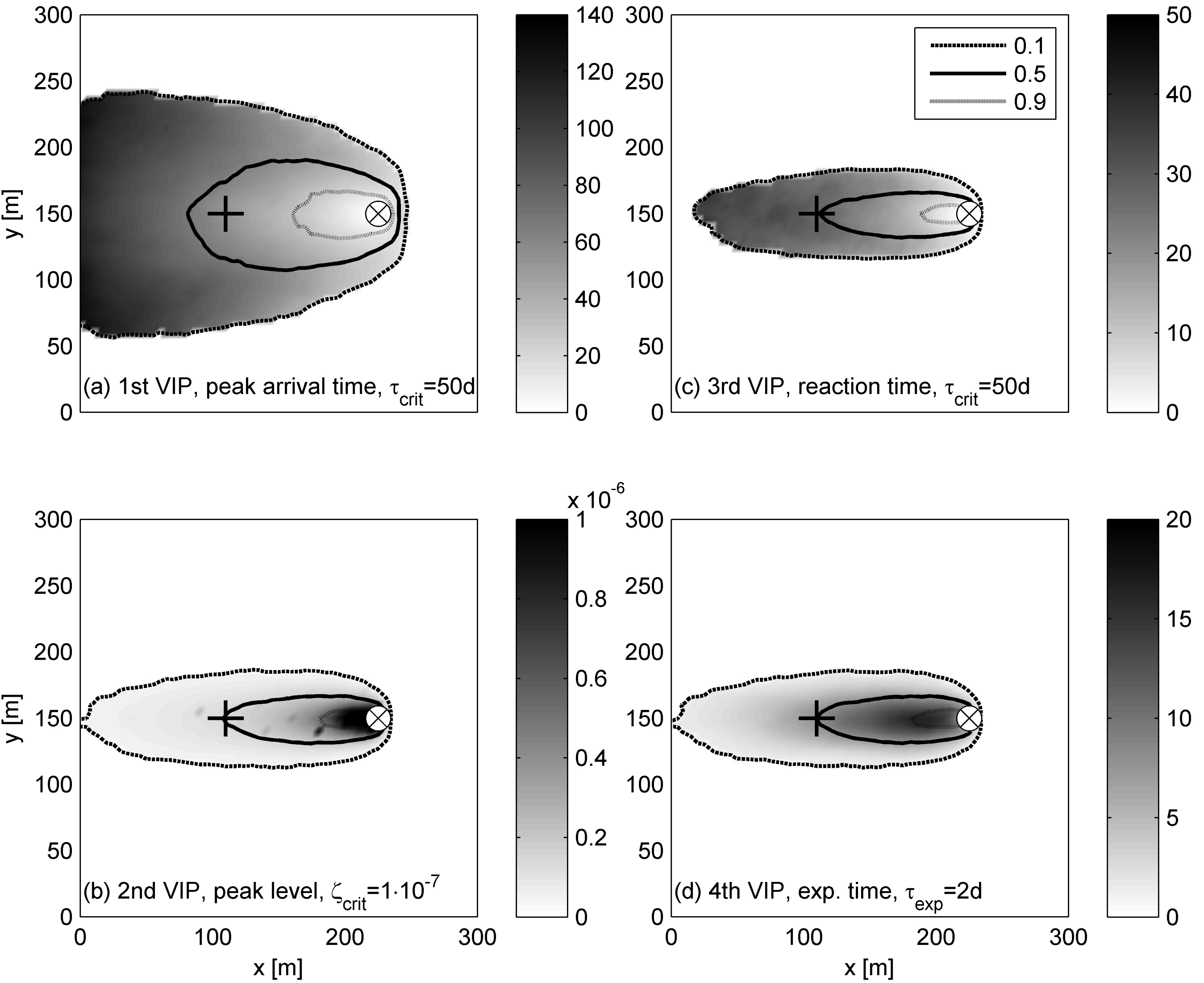

Figure 5
Click here to download Figure: Fig5observed.eps

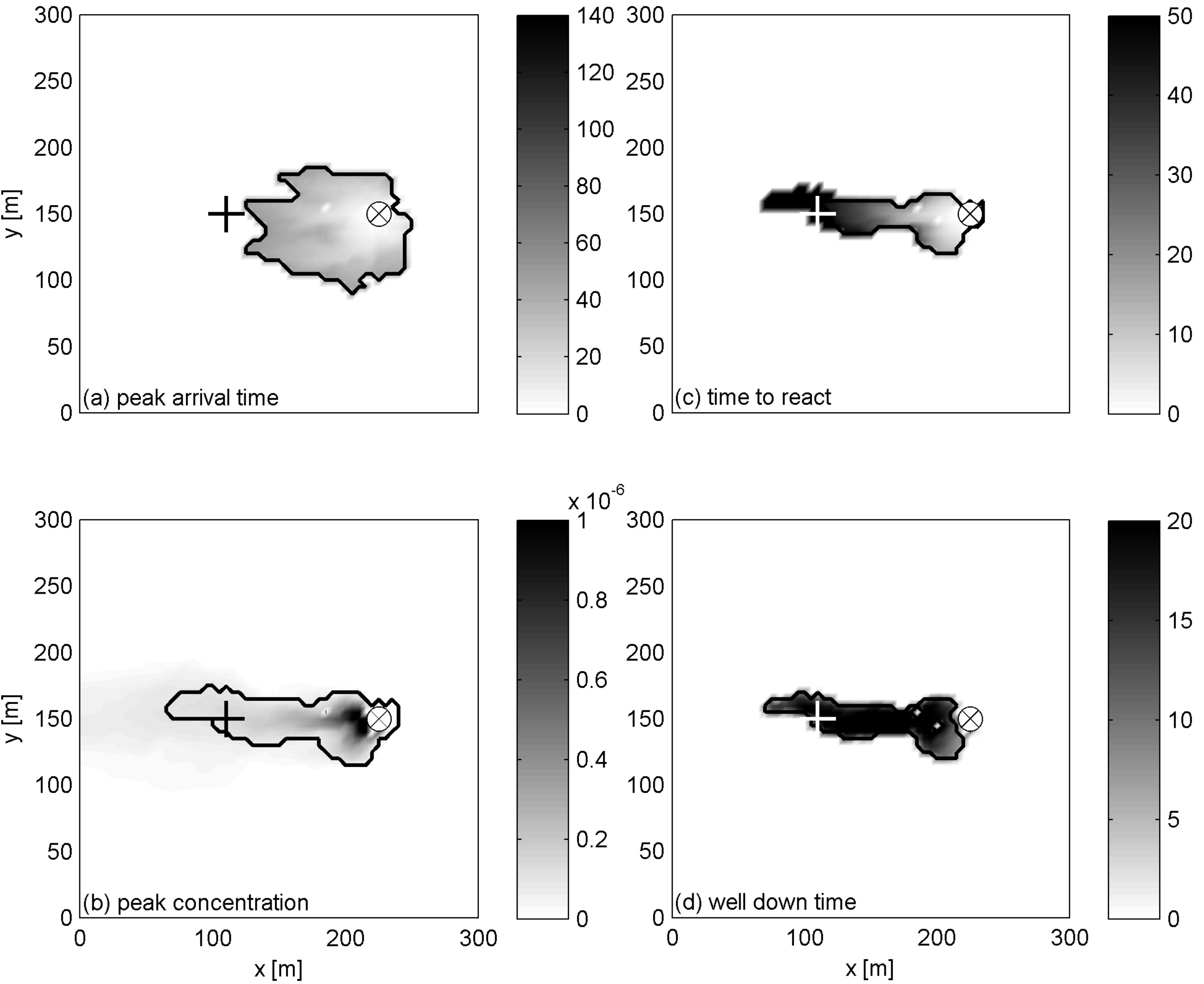

Figure 6

Click here to download Figure: Fig6cond.eps

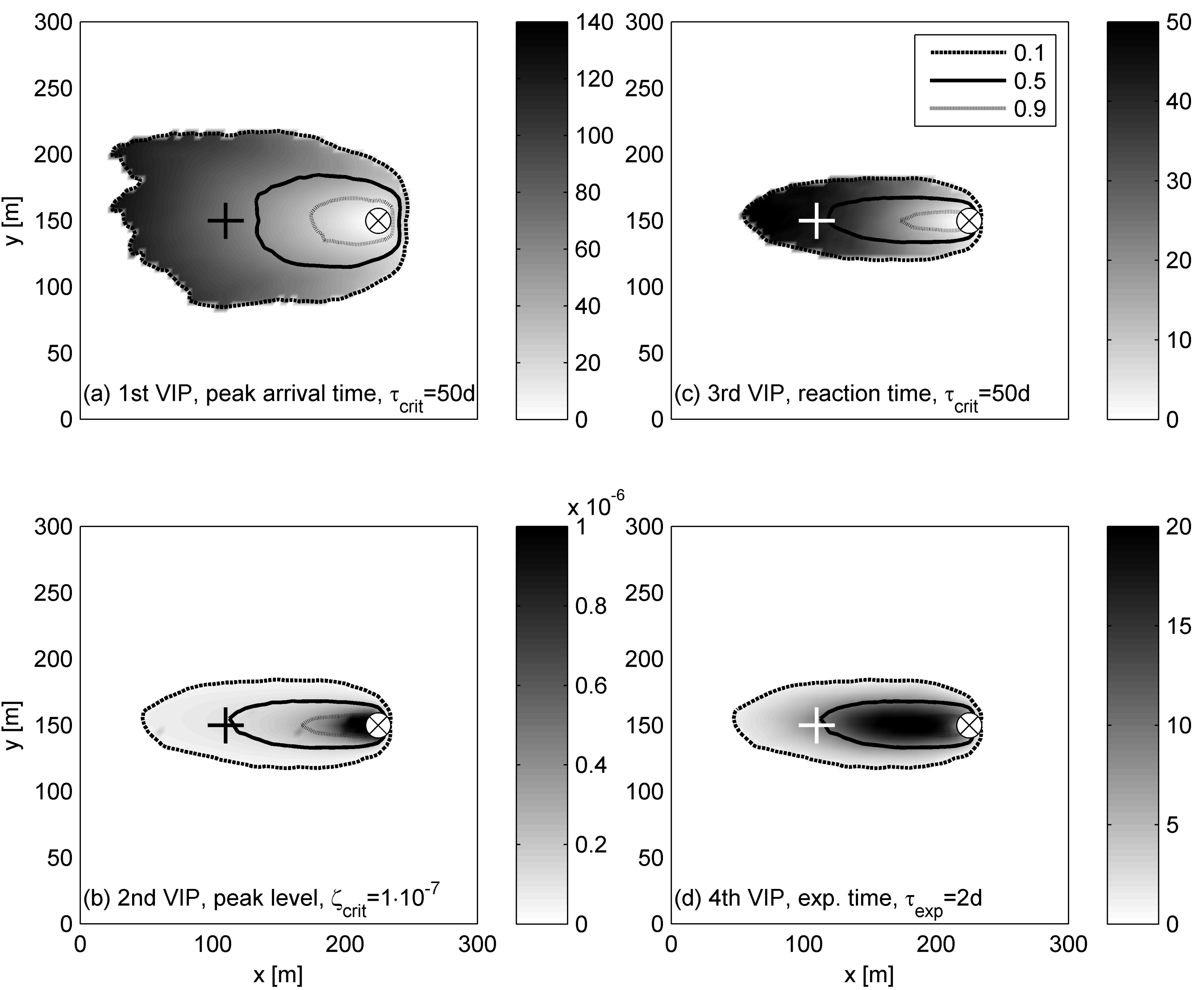

Figure 7
Click here to download Figure: Fig7_BTCall_uncond.eps

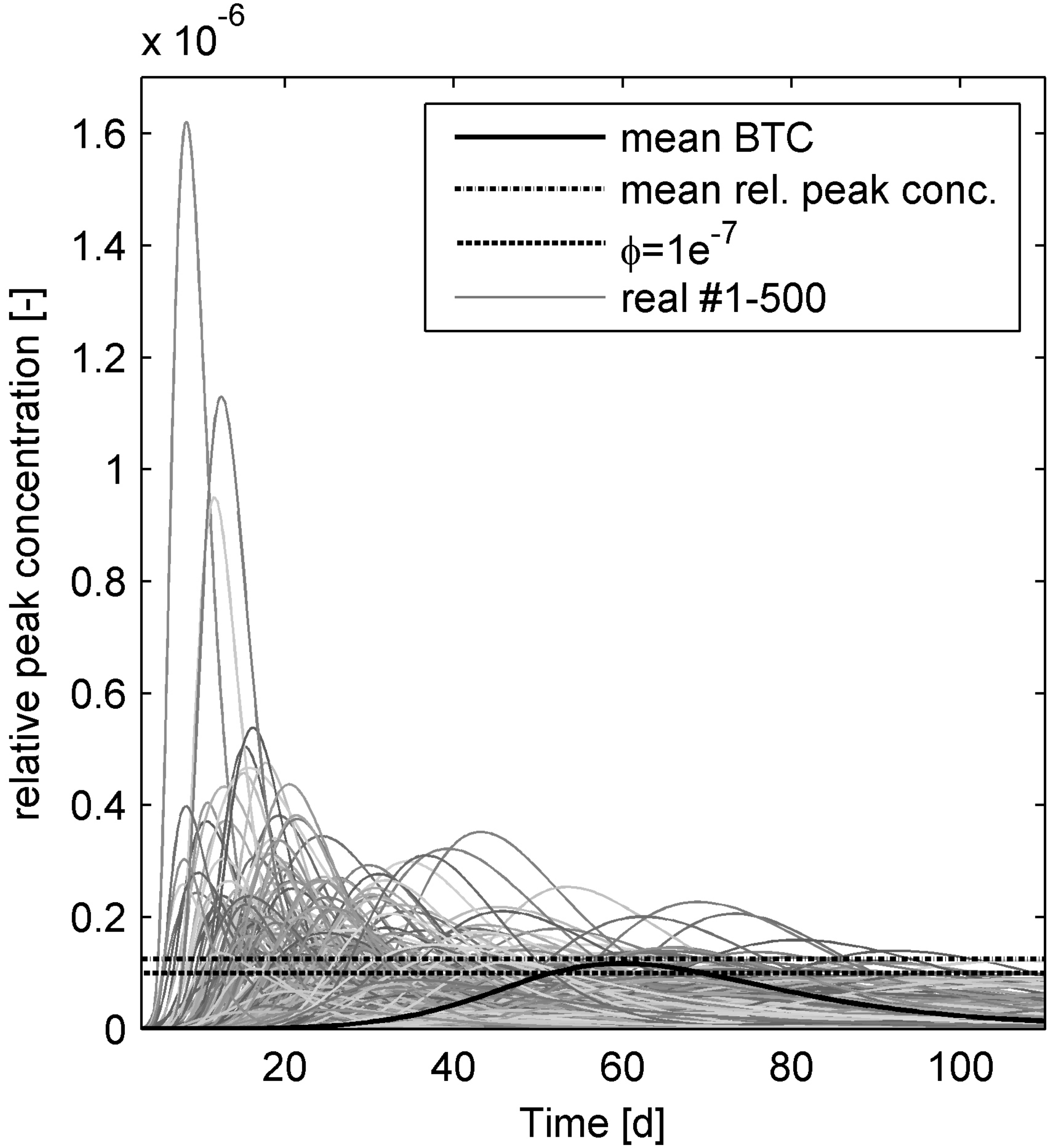

Figure 8a
Click here to download Figure: Fig8tpkct50_uncond.eps

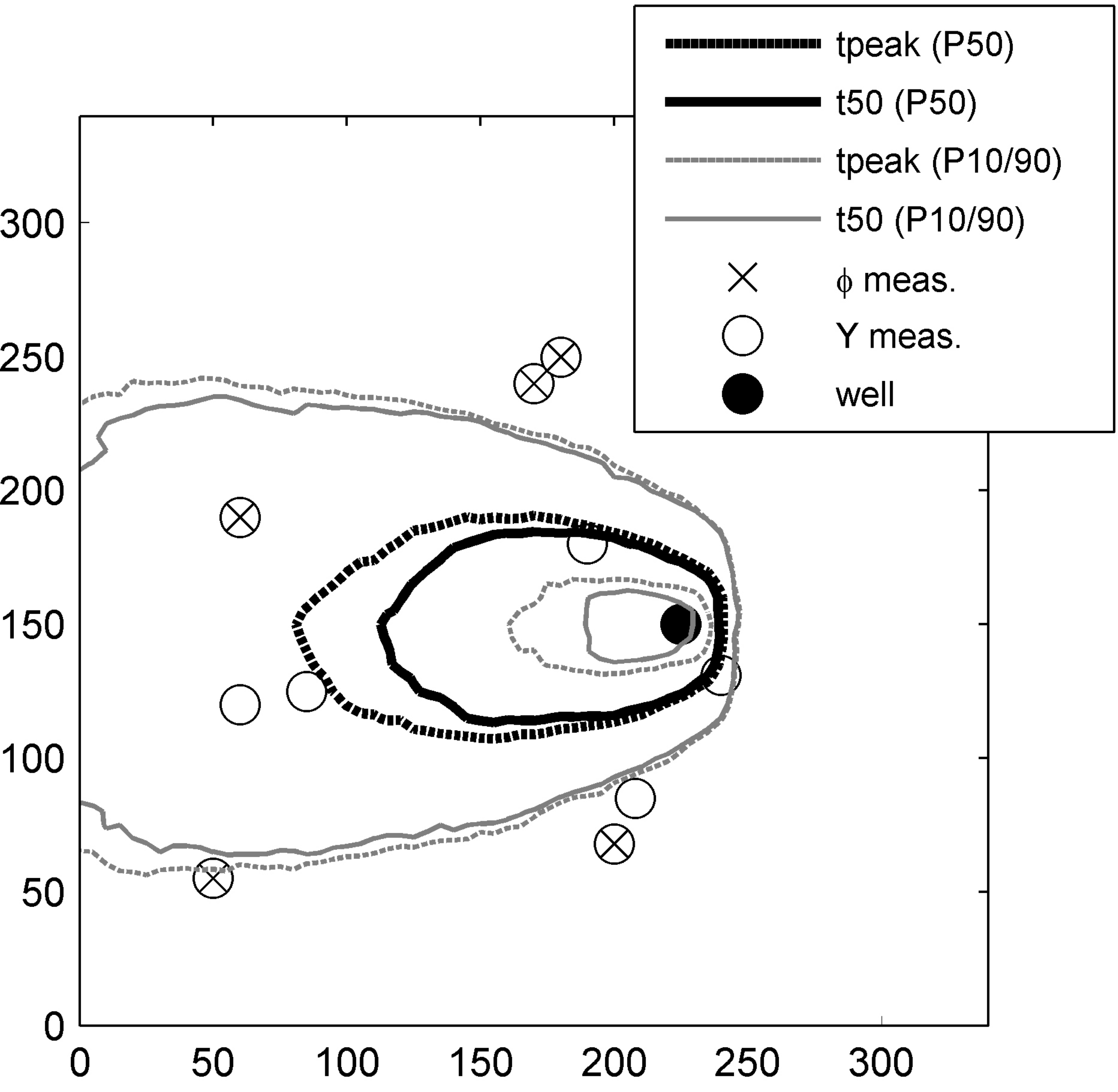

Figure 8b
Click here to download Figure: Fig8tpkct50_cond.eps

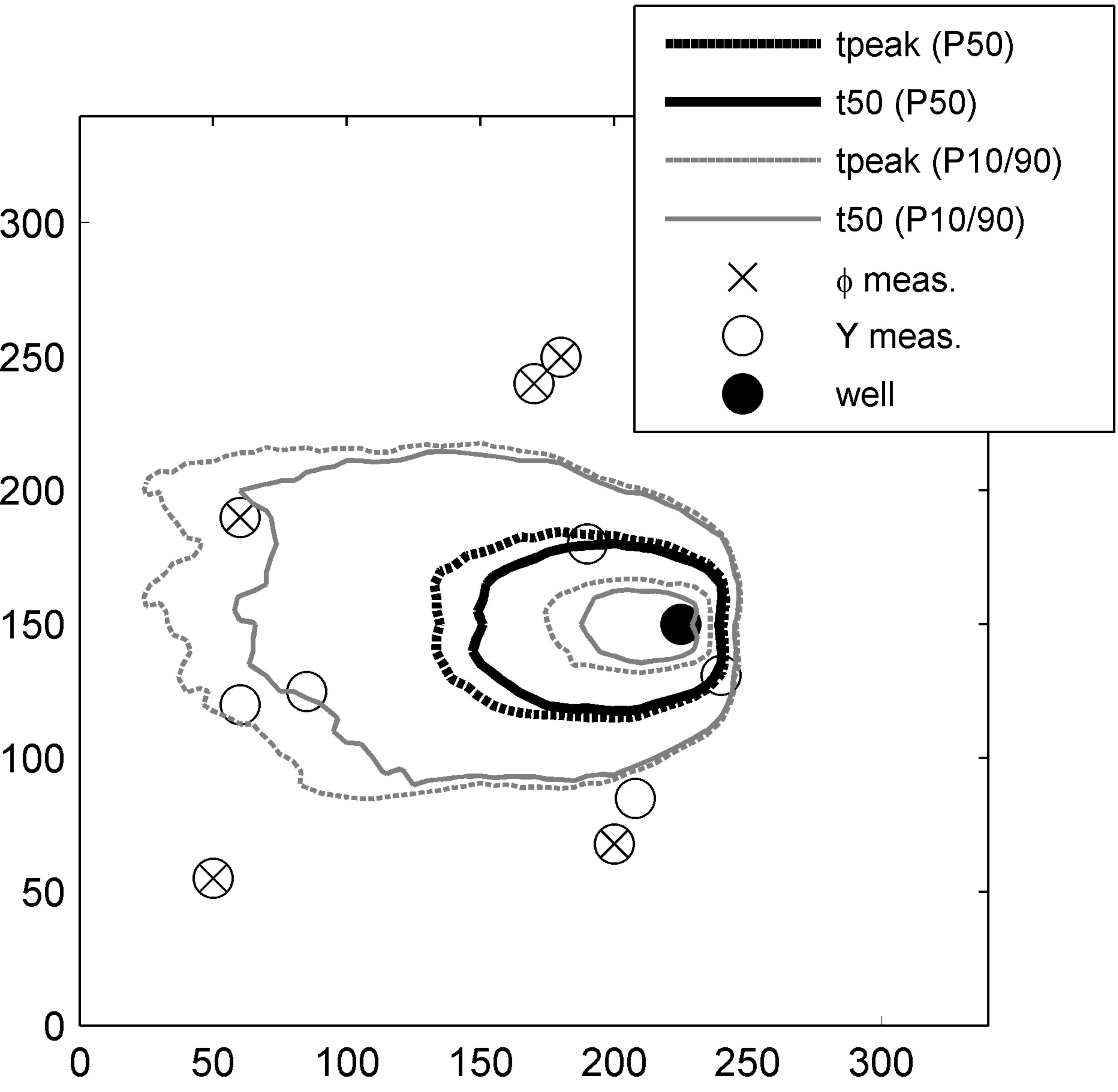

Figure 9
Click here to download Figure: Fig9tscat_uncond.eps